Testing Comptonizing coronae on a long *Beppo*SAX observation of the Seyfert 1 galaxy NGC 5548

P.O. Petrucci[1,2], F. Haardt[2], L. Maraschi[1], P. Grandi[3], G. Matt[6], F. Nicastro[3,4,5], L. Piro[3], G.C. Perola[6], A. De Rosa[3].

Received _____; accepted _____

[1]Osservatorio Astronomico di Brera, Milano, Italy

[2]Universitá dell'Insubria, Como, Italy

[3]IAS/CNR, Roma, Italy

[4]CfA, Cambridge Ma., USA

[5]Osservatorio Astronomico di Roma, Roma, Italy

[6]Universitá degli Studi "Roma 3", Roma, Italy

ABSTRACT

We test accurate models of Comptonization spectra over the high quality data of the *Beppo*SAX long look at NGC 5548, allowing for different geometries of the scattering region, different temperatures of the input soft photon field and different viewing angles. We find that the *Beppo*SAX data are well represented by a plane parallel or hemispherical corona viewed at an inclination angle of 30°. For both geometries the best fit temperature of the soft photons is close to 15^{+3}_{-9} eV. The corresponding best fit values of the hot plasma temperature and optical depth are $kT_{\rm e} \simeq$ 250–260 keV and $\tau \simeq 0.16$–0.37 for the slab and hemisphere respectively. These values are substantially different from those derived fitting the data with a power-law + cut off approximation to the Comptonization component ($kT_{\rm e} \lesssim$ 60 keV, $\tau \simeq 2.4$). In particular the temperature of the hot electrons estimated from Comptonization models is much larger. This is due to the fact that accurate Comptonization spectra in anisotropic geometries show "intrinsic" curvature which reduces the necessity of a high energy cut-off. The Comptonization parameter derived for the slab model is larger than predicted for a two phase plane parallel corona in energy balance, suggesting that a more "photon-starved" geometry is necessary. The case of a hemispheric corona is consistent with energy balance but requires a large reflection component. The spectral softening detected during a flare which occurred in the central part of the observation corresponds to a decrease of the Comptonization parameter, probably associated with an increase of the soft photon luminosity, the hard photon luminosity remaining constant. The increased cooling fits in naturally with the derived decrease of the coronal temperature $kT_{\rm e}$ in the high state.

Subject headings: radiation mechanisms: thermal; galaxies: active; galaxies: individual(NGC 5548)

1. Introduction

The X-ray emission of Seyfert galaxies is commonly believed to be produced by Compton scattering of soft photons on a population of hot electrons (Pozdniakov et al., 1976; Shapiro et al., 1976; Liang & Price, 1977; Sunyaev & Titarchuk, 1980). Although high energy observations of Seyfert galaxies may be consistent with both thermal and non–thermal models (Zdziarski et al. 1994; Malzac et al. 1998) the non–detection of Seyferts by Comptel and the high energy cut-offs indicated by OSSE (Jourdain et al. 1992; Maisack et al., 1993) and *Beppo*SAX (Matt 1999) have focused attention on thermal models. In fact it was shown early on that assuming thermal equilibrium and a plane parallel geometry for the Comptonizing plasma above an accretion disk, and neglecting direct heating of the disk, the average properties of the X-ray emission of Seyfert galaxies could be naturally accounted for (Haardt & Maraschi 1991). The spectral slope is mainly determined by two parameters, the temperature $kT_{\rm e}$ and optical depth τ of the scattering electrons, while the cut–off energy is related essentially to kT_e. Thus, simultaneous measurements of the slope of the X-ray continuum *and* of the cut–off energy are necessary to determine the physical parameters of the Comptonizing region.

Moreover, in a disk plus corona system, the Comptonizing region and the source of soft photons are *coupled*, as the optically thick disk necessarily reprocesses and reemits part of the Comptonized flux as soft photons which are the seeds for Comptonization. The system must then satisfy equilibrium energy balance equations, which depend on *geometry* and on the ratio of direct heating of the disk to that of the corona. In the limiting case of a "passive" disk, the amplification of the Comptonization process, determined by the Compton parameter $y \simeq 4\left(\frac{kT_e}{m_e c^2}\right)\left[1+4\left(\frac{kT_e}{m_e c^2}\right)\right]\tau(1+\tau)$, is fixed by geometry only. Therefore, if the corona is in energy balance, the temperature and optical depth must satisfy a relation which can be computed for different geometries of the disk+corona configuration (e.g., the review of Svensson 1996). It is then theoretically possible to constrain the geometry of the system and verify the selfconsistency of the model, provided that kT_e and τ are known with sufficient precision.

The extent of spectral variability during luminosity variations is an additional, in principle powerful, diagnostic tool that can be used to test existing models, as it provides direct insight into the way the emitting particles are heated and cooled. For example, if the plasma is pair dominated, the value of τ is fixed by the compactness parameter (i.e. by the luminosity for fixed geometry). This yields a definite relation between spectral variations and intensity, predicting modest spectral changes for large (factor 10 at least) variations in the intensity. On the contrary, for low pair density plasmas, significant spectral variations are possible

even in the absence of luminosity variations. In the latter case, for constant geometry (i.e. at a constant Compton parameter y), the spectral index is expected to increase when the electron temperature decreases (Haardt, Maraschi & Ghisellini 1997).

In the present paper, our aim is to test Comptonization models over high quality data, deriving further constraints on the physical parameters and geometry of the source. To achieve such goal, the long look at the Seyfert I galaxy NGC 5548 performed by *Beppo*SAX provides an ideal dataset. Previous studies of the source conducted over several years using EXOSAT, GINGA, ASCA and RXTE and, in some cases, coordinated observations first with IUE and later with EUVE (Walter & Courvoisier, 1990; Nandra et al., 1991; Chiang et al., 2000) support the general Comptonization picture, revealing the presence of several components in the X-ray spectra (neutral Iron line, reflection hump, soft excess...). No information on the high energy and of the Comptonization component could however be obtained from the above studies. Magdziarz et al. (1998), using average OSSE data and non simultaneaous GINGA observations, suggested a temperature of 50 keV for the hot corona.

NGC 5548 was observed by *Beppo*SAX in a single long (8 days) observation, with a net exposure of 314 ks on source. The high quality of the *Beppo*SAX data allows a detailed study of the spectrum over a very wide energy range, from 0.2 to 200 keV, and offers the opportunity to study spectral variability, since a conspicuous flare occurred in the middle of the observation. A detailed analysis of these data has been presented by Nicastro et al. (1999, hereafter N99). The differences between the latter analysis and our results concern only the modelling of the continuum and will be discussed in the course of the paper.

Our main progress here is to adopt and fit directly to the data a detailed model of the Comptonized spectrum, for which the commonly adopted representation of a simple power law with a high energy cut–off turns out to be a rather poor approximation. Effectively, Comptonized spectra intrinsically show additional features, such as bumps due to different scattering orders, and an anisotropy "break" due to the (plausible) anisotropic nature of the soft photon input.

The paper is organized as follows. In section 2 we briefly summarize the main characteristics of Comptonization models, and compare results of different approaches and geometries. The analysis of the *Beppo*SAX data is presented in section 3. We will not be concerned here in detail with the warm absorber features already discussed in N99. In section 4, we compare the *Beppo*SAX data with non–simultaneous IUE and OSSE data. We discuss our results and their physical interpretations in section 5. We then conclude in the last section.

2. The Comptonization Model

Theoretical Comptonized spectra, produced by a mildly relativistic plasma scattering off low–frequency radiation, have been computed for two decades now (Shapiro, Lightman & Eardley 1976; Sunyaev & Titarchuk 1980; Pozdnyakov, Sobol & Sunyaev 1976). More recently, it has been realized that, if the scattering occurs above an accretion disk, the source of seed photons is anisotropic, introducing anisotropies and modifications of the outgoing spectrum. Haardt & Maraschi (1991, 1993) and Haardt (1993) derived the angle–dependent spectra from disk–corona system using an iterative scattering method, where the scattering anisotropy was taken into account only in the first scattering order. Other more detailed works have followed, exploiting non linear Monte Carlo techniques (Stern et al 1995b), or the iterative scattering method (Poutanen & Svensson 1996, hereafter PS96), allowing the treatment of systems with different geometries such as slabs, cylinders, hemispheres, and spheres. All these works have shown that anisotropic effects are important, and indeed can modify substantially the spectral shape of the Comptonized radiation. The largest effect occurs when soft photons are emitted by a plane (disk) on one side of the corona. In this case, photons backscattered towards the disk in the first scattering are necessarily produced in "head–on collisions" and therefore have an energy gain larger than average, while photons scattered towards the corona (i.e. in the forward direction) have an energy gain smaller than average. As a consequence, the contribution of the first scattering order to the outgoing flux is significantly reduced. Clearly, this effect becomes important when the energy gain per scattering is large, that is when kT_e is mildly relativistic, say $kT_e \gtrsim 100$ keV.

In Fig. 1 we compare spectra computed for the same value of the coronal temperature (kT_e=360 keV) for different geometries. For the slab geometry, we show spectra obtained with the code of Haardt (1994, hereafter H94), whereas the hemispherical and the spherical ones have been produced by the code kindly made available by Poutanen & Svensson (PS96). We have checked that in the slab case the two codes give identical results. For the sphere, the soft photons are supposed to be emitted isotropically at the centre of the sphere, whereas they come from the bottom for the slab and the hemisphere configurations. In each case, the optical depths have been chosen so as to produce approximatively the same spectral index in the X–ray range. We have thus taken τ=0.09, 0.16 and 0.33 for the slab, hemisphere and sphere geometry, respectively. We have also plotted, for comparison, a cut–off power law spectrum setting the e–folding energy $E_{\rm c} = 2kT_{\rm e}$=720 keV, as a first order approximation to Comptonization spectral models (for $\tau \lesssim 1$).

It is clear, from Fig. 1, that the spectra are quite different at medium - high energy ($E \gtrsim 10$ keV). Below the high energy cut–off the spectra for the slab and hemisphere cases can be approximately described by

broken power laws. The slope observed at low energies is harder due to the deficiency of once scattered photons. In this range the spectral index depends on the viewing angle, since the anisotropy is maximal at 0 degrees. The slope *above the break* corresponds to that produced by the Comptonization process without taking into account anisotropy and is therefore almost angle–independent.

The energy of the break $E_{\rm break}$ should approximately correspond to the peak energy of the spectrum formed by twice–scattered photons. In practice $E_{\rm break}$ is close to the peak energy of the third scattering order (Haardt 1993), that is (assuming a black body soft emission):

$$E_{\rm break} \simeq 2.7 kT_{\rm bb} \left[16 \left(\frac{kT_e}{m_e c^2} \right)^2 + 4 \left(\frac{kT_e}{m_e c^2} \right) + 1 \right]^3 . \quad (1)$$

In cases relevant for Seyfert galaxies, $E_{\rm break}$ is typically of the order of few keV, much lower than the high energy cut–off. The anisotropy break is thus an important feature when fitting real data, even if it may be hidden by the presence of the reflection hump above 10 keV.

The anisotropy break is important only for high temperatures. In fact, for $kT_e \lesssim 50$ keV, the forward–backward anisotropy becomes small and consequently, the amplitude of the spectral break decreases. Also, for small values of τ, a broken power law is not a good description of the emerging spectrum anyway, since the spectrum is formed by distinct humps corresponding to the different Compton scattering orders. Finally, for high values of $kT_{\rm bb}$, as may be the case for galactic black holes, $E_{\rm break}$ can be well above 10 keV, completely hidden by the reflection component.

For the same temperature, a hemispheric geometry gives rise to a larger anisotropy (larger break) than a slab. This can be qualitatively understood as follows. Consider a pole on observer and the seed photons emitted at the centre of the bottom of the hemisphere. In the first scattering order all scattering angles between 0 and 90 degrees (final direction towards the pole on observer) have similar probabilities. In the slab case the scattering at 90 degrees has larger probability relative to that at 0 degrees since the optical depth along the horizontal direction is larger than along the vertical.

Note that the shape of the break has important effects on the best–fit values of other parameters involved in the fitting procedure. For instance, we expect that the amplitude of the reflection component derived from the spectral fit when allowing for an anisotropy break in the continuum will be larger for configurations with larger anisotropy and minimal in the case of a simple power-law model (cf. Table1).

3. Application of different models to the *Beppo*SAX data of NGC 5548

Here we will be concerned with data from three instruments on board *Beppo*SAX : the Low Energy Concentrator Spectrometer, LECS (Parmar et al. 1997) covering the 0.15–10 keV range, the Medium Energy Concentrator Spectrometer, MECS (Boella et al. 1997) covering the 2–10 keV range and the Phoswich detector system, PDS (Frontera et al. 1997) covering the range 12 – 200 keV. For a description of the instruments and data reduction procedure we refer to N99 and references therein.

A careful analysis of the *Beppo*SAX data was carried out by N99. The continuum, was described using a simple cut–off power law model

$$f_E \propto E^{1-\Gamma}\, \mathrm{e}^{-E/E_\mathrm{c}}, \tag{2}$$

characterized by the photon index Γ, and the e–folding energy E_c, with additional, superimposed features due to reflection and the possible presence of a warm absorber. The source brightened during the central ∼70 ks of the observation by ∼30% in the LECS and by ∼15% in the MECS. No significant variability larger than ∼ 20% was detected in the 13–200 keV PDS range. N99 divide the observations into three parts, each with nearly constant intensity and with similar signal to noise ratio: two low states L1, L2 (from the first ∼ 120 ks and the last ∼ 106 ks of the observation respectively) and a high state H (from the central ∼ 70 ks of the observation). The main results of N99 can be summarized as follows:

- the average spectral data can be well fitted by a cut–off power law, plus reflection component and warm absorber features. For most of the duration of the observation (i.e. in the low state), the continuum is characterized by $\langle\Gamma\rangle = 1.59$ and $E_\mathrm{c} = 115$ keV
- NGC 5548 shows significant spectral variability between the low and high states, with $\Delta\Gamma \simeq 0.2$ (the low state being the harder one), whereas the total luminosity remains essentially constant. The high energy cut-off is also tightly constrained in the low state, $E_\mathrm{c} = 115^{+39}_{-27}$ keV, while, in the high state, a lower limit is obtained, $E_\mathrm{c} \gtrsim 260$ keV. This lower limit is however larger than the one obtained in the low state.
- the presence of a warm absorber in this source is confirmed, and for the first time an emission feature, possibly associated with the OVII-OVIII Kα and K$_\beta$ emission lines at ∼0.6 keV, is detected.

Here we focus on the continuum plus reflection components fitting directly Comptonization spectra computed for different values of the physical parameters kT_{bb}, τ and kT_e and for different geometries. In our

analysis, we used the H94 and PS96 codes. The advantage of the H94 code is that its outputs are computed before the fitting procedure, and stored as a table in XSPEC, so that searching for best fit values, confidence levels, errors, etc, is a very fast procedure. For this reason, throughout the paper, fits to the slab model always refer to the H94 code outputs, while for the hemisphere and sphere geometries the results reported have been obtained using the PS96 code.

The reflection component was included following White, Lightman & Zdziarski (1988) and Lightman & White (1988) and assuming neutral matter. In the H94 code, a constant spectral shape averaged over angles is assumed for the reflected photons. It is multiplied by a normalization factor which depends on the inclination angle (see Ghisellini, Haardt & Matt 1994 for details). PS96 instead computes the reflection component for the given inclination angle using the Green functions of Magdziarz & Zdziarski (1995). The geometrical normalization of the reflection component R is left as a free parameter. A value $R = 1$ corresponds to a covering factor of the cold matter to the X–ray source of $\Omega = 2\pi$. Note that the X–ray emission, as discussed in Section 2, is not assumed to be isotropic.

The iron line is modeled by a Gaussian with null width, since the line appeared practically unresolved ($\sigma_{F_e} < 300$ eV) in the previous analysis of N99. The central energy of the line is fixed at 6.3 keV, the best fit value obtained by N99. For what concerns the warm absorber (WA), we simply modelled it as two edges at 0.74 and 0.87 keV, to account for O VII and O VIII absorption. A more detailed analysis, as that done by N99, is beyond the scope of our paper, which is instead focused on the high energy continuum. We have however checked that a better modelization of the WA (CLOUDY code used by N99) does not affect the results obtained in this paper.

Finally, the LECS/MECS and PDS/MECS normalization ratios were frozen to the standard values of 0.75 and 0.88 respectively (Fiore, Guainazzi & Grandi 1999). The results of the fits are detailed in the following sections. Throughout the paper, errors on single parameter (obtained by letting the others free to vary) are quoted at a confidence level of 90 % (i.e. $\Delta\chi^2$=2.7) unless otherwise specified.

3.1. Constraining the soft photon field and the inclination angle

To take advantage of the maximum available signal to noise ratio, we consider first the total data set obtained by *Beppo*SAX , that is the average over the whole observation period from the three Narrow Field Instruments, LECS, MECS and PDS. These data taken together cover the range from 0.15 to 200 keV.

We start to constrain the values of the soft photon temperature $kT_{\rm bb}$, and of the inclination angle i (or its cosine $\mu \equiv \cos i$). To this end we assume a fixed, slab geometry where the input soft radiation field is supposed to be localized on one side of the slab.

A soft X–ray excess was found previously in NGC 5548 (Done et al. 1995; Magdziarz et al. 1998), but is not present in the *Beppo*SAX spectra (N99). From IUE data, the UV bump seems to peak above 3 eV (Clavel et al. 1992; Magdziarz et al. 1998). We therefore tested values of $kT_{\rm bb}$, in the 5 to 50 eV range.

We perform a best–fit analysis on the four parameters $kT_{\rm bb}$, kT_e, τ and R with two fixed values of μ. The results of the fitting procedure are reported in Table 1, where we give the best fit values and 90% confidence errors for each of the four fitted quantities.

For an inclination angle of 30° the best fitting soft temperature $kT_{\rm bb}$ is 16 eV, with a 90% confidence interval between 7 and 18 eV. This is higher but not far from the maximum temperature deduced from the UV spectrum suggesting that the emission from the accretion disk should extend to higher energies. This could be due to deviations from a pure blackbody emission and/or to the presence of a hotter inner region of the disk. The reflection component is nicely consistent with a solid angle of 2π. High black body temperatures (20 eV and larger) are statiscally unacceptable. The reason is that, in these cases, the high energy tail of the UV–to–Soft–X-ray bump would fall in the LECS band.

It is worth stressing, at this point, that the *Beppo*SAX data, as already noted by N99, do not confirm the presence of a soft excess, as observed by ROSAT in 1992-1993 (Done et al. 1995). This discrepancy could be due to systematic errors in the ROSAT low energy data, as already discussed by Iwasawa et al. (1999) but may also result from a possible variability of the soft component. In the latter case the soft photon temperature could be different at different epochs. We recall that the soft excess derived by Reynolds (1997), fitting ASCA data of NGC 5548, having best fit black body temperature of 240 eV, referred to a state when the spectral index of the continuum was 1.9, definitely steeper than during this *Beppo*SAX observation (see further discussion section 5.2).

For a larger inclination angle, $i = 60°$, the fit yields a smaller value of the reflection component R. This is because the anisotropy of the Compton emission is maximum at $i = 0°$, and is reduced for increasing inclination. Hence the difference in spectral index before and after $E_{\rm break}$ is smaller for i= 60°. The MECS data constrain the spectral index for $E \lesssim E_{\rm break}$, leaving, for larger viewing angles, less room for the reflection component, which peaks at energies $E \gtrsim E_{\rm break}$. Figure 2 shows the LECS, MECS and PDS spectra and the best fit models obtained with inclination angles of 30° and 60° respectively. Although the χ^2 value is

acceptable in both cases, it is significantly worse for the larger angle ($\Delta\chi^2$=35) as shown by the fit residuals in the PDS range. We will not discuss the inclination further fixing $i = 30°$ in the following.

The χ^2 contour plots for two parameters (confidence levels of 68%, 90%, and 99%) for slab models with $i = 30°$ are shown in Fig. 3. The joint confidence levels of kT_e and τ is shown in Fig. 3c. To compute these contour plots kT_{bb}, τ, kT_e, R and the model normalization were allowed to vary, while the Fe line intensity and the depth of the Oxygen edges were frozen to their best fit values, since they do not significantly affect the fit of the continuum. From such plot one can see how kT_e and τ adjust so that the combination of the two produces a spectrum with the observed shape. In fact the shape of the contours follows approximately a line of constant Comptonization parameter.

3.2. Comparing different geometries

In order to test different geometries we performed spectral fits using the PS96 code for a hemisphere with soft photon input from the bottom plane and a sphere with soft photons isotropically emitted at the centre. In the first case the fits were performed for different values of the inclination angle as previously done for the slab case. Again the best quality fits are obtained for $i = 30°$. The results are reported in Table 1. In both cases the derived temperature of the hot Comptonizing electrons does not change significantly with respect to the case of the slab geometry. The optical depth adjusts as expected towards somewhat higher values, since for the slab configuration the optical depth parameter, which is measured in the vertical direction, is lower than the average optical depth seen by the Comptonized photons. The soft photon temperature for the hemisphere model also coincides with that for the slab, while it is somewhat lower in the case of the sphere. The largest difference is the value of the reflection component, which is larger for larger anisotropy. In fact the hemisphere yields the largest value and the sphere the smallest one (cf. section 2).

We also report in Table 1 the best fit parameters of a simple cut–off power law (plus reflection) model (PEXRAV model in XSPEC, Magdziarz & Zdziarski 1995). For this model, the fit parameters are the e–folding energy of the cut–off power law $E_{\rm c}$, the photon index Γ and the reflection normalization R. Note that our best fit values are in complete agreement with those obtained by N99. On the other hand, here and in the following sections, we report "equivalent" values of kT_e also for PEXRAV, simply computed as $kT_e \equiv E_{\rm c}/2$, keeping in mind that such approximation roughly holds for $\tau \lesssim 1$. For $\tau \gg 1$, $kT_e \equiv E_{\rm c}/3$ would be more appropriate. The value reported can be considered as an upper limit to the temperature estimated from a cut–off power law model. Knowing the temperature, the spectral index derived from the PEXRAV fit can

be used to determine the optical depth using the relation (Shapiro, Lightman & Eardley 1976; Sunyaev & Titarchuk 1980; Lightman & Zdziarski 1987):

$$\Gamma - 1 = \left[\frac{9}{4} + \frac{m_e c^2}{kT_e \tau(1+\tau/3)}\right]^{1/2} - \frac{3}{2} \tag{3}$$

This equation is valid for $\tau \gg 1$, and we have checked *a posteriori* that such condition is roughly matched in all cases.

Every alternative geometry gives statistically acceptable fits. The spherical (isotropic) model, though acceptable, is however considerably worse than the others. Also it is surprizing that the best fit temperature obtained with this model is similar to the anisotropic models rather than to the PEXRAV results. We therefore checked this result fitting the data with the analytical Comptonization model of Titarchuck (COMPTT model of XSPEC, Titarchuk 1994) and adding the reflection component computed by PEXRAV, a gaussian for the iron line and two edges for the O VII and OVIII ones. Such model should represent quite well the case of an isotropic spherical geometry. The best fit then gives $\tau \simeq 4.3$ and $kT_e \simeq 30$ keV, comparable to the PEXRAV results if $kT_e \simeq E_c/3$. We believe that the discrepancy with the results obtained using the spherical code of Poutanen is due to the fact that the latter is limited to $\tau \leq 3$ (we have cheked that both codes are in agreement when we fixed τ to 3). This can prevent the fitting procedure to find an acceptable fit with low temperature and high optical depth. We therefore will not discuss the spherical model further.

The data and best fit model for the hemisphere are compared in Fig. 2 with those for the slab. In Fig. 4, we show the confidence levels for various combinations of the fitted parameters (here again only kT_{bb}, τ, kT_e, R are allowed to vary) for the hemisphere configuration for an inclination angle fixed at 30°. In particular the contour plots of kT_e and τ for the hemisphere do not overlap those for the slab. Although the temperature range is the same, the optical depth is higher, yielding a larger value of the Comptonization parameter.

The theoretical relation between kT_e and τ expected for the slab and hemisphere configurations in energy balance and with negligible disk heating as computed by Stern et al. (1995a) are also shown on the same figures. The parameters derived for the slab correspond to a Comptonization parameter $y \simeq 1$ higher than expected in an equilibrium configuration ($y \simeq 0.5$). The case of a hemisphere appears in better agreement with the theoretical predictions from energy balance requirements. For the latter model the normalization of the reflection component is however relatively large (R = 1.6 ± 0.3) in marginal agreement with the measured EW (of the order of 120 eV) of the Fe line (George & Fabian 1991; Matt et al. 1991; Reynolds, Fabian & Inoue 1995). Thus neither model is entirely satisfactory. This problem will be further discussed

in section 5.

The most important and general conclusion from this section is that the temperature estimates of the hot electrons derived from fits with Comptonization spectra, irrespective of geometry, are substantially different from those obtained using models involving a power law with high energy cut–off plus a reflection component, exemplified by PEXRAV fits (see Table 1 and 2). This is due to the fact that the power law slope is determined with small errors by the LECS and MECS data. Since within PEXRAV type models this slope by hypothesis cannot change at higher energies, a cut–off around 100 keV is required to fit the PDS data. In Comptonization models, the LECS and MECS data determine the slope below the anisotropy break. Above this break the intrinsic spectrum is steeper and thus can fit the PDS data without an additional steepening below 100 keV, allowing for a larger temperature. The large difference in the fitted temperatures leads to widely different predictions as to the fluxes emitted at higher energies, above the PDS range.

3.3. Comparing the low and high states

We now discuss the spectral variations associated with the flare experienced by NGC 5548 during the central ∼70 ks of the *Beppo*SAX observation. Using direct Comptonization fits we can derive the variations of the physical parameters during the flare. Since no significant variations were found by N99 between the two low state spectra (before and after the flare), we combined them into a mean low state spectrum, labelled as "L". The high state spectrum will be referred to as "H". Again, we fixed the inclination at 30° and performed the fitting procedure for the plane parallel and hemispherical geometries for the two states.

The fits to the L and H spectra are shown in Fig. 5. The high quality of the data allows to constrain quite precisely the main parameters kT_{bb}, τ, kT_e and R in the two states. The best fit values are reported in Table 2, with their associated 90% error and confidence level contours are shown in Fig 6. While these errors take into account the possible variations of all the parameters involved, we stress that not all the parameters are expected to vary simultaneously. To illustrate the mutual parameter dependence we also show in Fig 6c the contour plots obtained assuming that the soft photon temperature remained constant during the flare. These "partial" contours suggest that for constant $kT_{\rm bb}$ the change in physical parameters is essentially a decrease of the coronal temperature. This is even more true if $kT_{\rm bb}$ *increases* in the softer state as indicated by the best fit values and discussed in section 5.2. We have reported the values of kT_e and τ found for the low and high states for the slab and hemisphere configuration in Fig. 7. Two main points should be noted here:

- the change of state of the source, from L to H, is consistent with a constant Compton parameter y. The trend in the $\tau - kT_e$ plane is for a decrease of the temperature of the hot corona in the high state, with a roughly constant optical depth.

- As the high state is the softer one (cf. Table 2), the temperature kT_e and the slope of the intrinsic continuum are anticorrelated, as expected if an increase of the cooling caused the hard–to–soft luminosity ratio to decrease.

We also derived values of kT_e and τ for both the low and high states using the slopes and cut–off energies obtained from fits with PEXRAV (see section 3.2) . These are reported in Table 2 and shown in Fig. 7. The errors on the temperature are rather large, since in this kind of model it is derived from the cut off energy which is constrained only by the hard X-ray data. We recall that in N99, only a lower limit to the cut–off energy was obtained for the high state. Our results have somewhat tighter constraints because we have fixed the relative normalization of the instruments.

In contrast with the results obtained using anisotropic Comptonization the parameter variations derived fitting PEXRAV models suggest that:

- the change of state of the source is consistent with the Compton parameter remaining constant during the transition but the trend in the $\tau - kT_e$ plane is for an increase of the temperature of the hot corona in the high state, with a decrease of the optical depth.

- the temperature of the corona is thus positively correlated with the continuum spectral index.

Thus not only different continuum models yield different values of the physical parameters but also the variability trends derived are opposite.

4. Multifrequency SED using non simultaneous IUE and OSSE data

Our purpose here is to examine whether existing data on the broad band energy distribution (optical to hard X–ray) may provide additional constraints to the Comptonization models discussed above. We therefore compare the *Beppo*SAX data on NGC 5548 to non–simultaneous UV and soft γ–ray data, obtained with IUE, and with OSSE on board *CGRO*, respectively. These data have been analysed, together with Ginga and ROSAT data, in Magdziarz et al. (1998, hereafter M98).

4.1. *UV data*

The ultraviolet spectra were extracted from the IUE electronic archive, and cover nine epochs, from January 1989 to July 1990. We use the data as reduced by M98. Emission lines were removed, and dereddened with E(B-V)$\simeq$ 0.03. The fit of the IUE data shown in Fig. 8 was done with an accretion disk model, consisting of multiple blackbody components, modified by the estimated absorption. In addition a vertical line represents the dispersion of the UV fluxes of NGC 5548 measured with IUE between 1983–1995 (see also Clavel et al. 1992). The best fit gives an inner disk temperature of $\sim$ 3 eV and a flux of $\sim 10^{-10}$ erg s^{-1} cm^{-2}. Note that the UV and X–ray luminosities appear to be of the same order. Moreover the extrapolation of the X-ray spectrum towards lower frequencies falls well below the peak of the putative disk emission. Although some caution is in order due to the non simultaneity of the observations and to the absence of data in the FUV – EUV range, this result is consistent with a) a corona with low optical depth and covering factor of order unity or b) a patchy corona with larger (> 1) local optical depth but which covers a small fraction of the surface which emits the thermal radiation.

4.2. *OSSE data*

The OSSE data were obtained during different observing periods in 1991 and in 1993 (See also M98). Their average was used to constrain the high energy cut-off by fitting simultaneously the *Beppo*SAX data with the OSSE data with a free relative normalization, which turns out to be 30% higher with respect to the MECS fluxes. Unfortunately, the OSSE data have a relatively poor signal–to–noise ratio, and their inclusion in the fit does not lead to an improvement in the determination of the temperature of the hot plasma. They clearly show however that the larger temperature estimated with the Comptonization models is completely consistent with the highest energy data available.

5. Discussion

5.1. Physical parameters of the corona

5.1.1. Temperature and optical depth

Thanks to the long *Beppo*SAX observation of NGC 5548, we were able to test quantitatively accurate anisotropic Comptonization models for the X-ray emission from this source. We have shown that if such

models are adopted, either in a plane parallel or hemispheric approximation for the geometry of the corona, the inclination angle should be low, $i \simeq 30^\circ$ and the soft photon temperature $kT_{\rm bb} \simeq$ 5-15 eV.

The best fit values of the hot plasma temperature and optical depth depend somewhat on the adopted geometry and on the state of the source, but in any case, *the estimated temperatures, $kT_{\rm e} \simeq$ 250 – 260 keV, are substantially larger than those inferred from fits with a cut–off power law.* N99 find a high energy cut–off $E_{\rm c}$ of the order of 120 keV, corresponding to a temperature $kT_{\rm e} \simeq 60$ keV (see also Table 2).

Correspondingly the optical depth, $\tau \simeq 0.16$–0.37 (for the slab and hemisphere geometry) is smaller than that deduced from the PEXRAV best fit where $\tau \simeq 2.4$. Large values of τ should have observable consequences on the profile of the Fe line component produced in the disk, leading to an attenuation and broadening of the line. At present the profile of this line in NGC 5548 is not unambiguously determined. The line seems unresolved in the *Beppo*SAX data (N99) but a significant width is suggested by ASCA data (Mushotzky et al., 1995; Nandra et al., 1997; Chiang et al., 2000; N99). Forthcoming observations with CHANDRA and XMM-Newton are expected to bring substantial progress on this issue.

We show in Fig.8 the best fit Comptonization model (in slab geometry) of the *Beppo*SAX data of NGC 5548, together with the best fit model obtained with a cut–off power law model (in solid and dashed line respectively). Due to the different normalization of the reflection component both models are in good agreement for $E \lesssim 100$ keV. Above this energy the two models diverge, the first one predicting much larger fluxes. Unfortunately the available non–simultaneous OSSE data cannot discriminate between the two. This underlines the need of better soft γ–ray observations, as those possibly provided by INTEGRAL, in order to directly confirm or disprove the temperatures inferred with anisotropic Comptonization models.

5.1.2. Energy Balance

The physical parameters $kT_{\rm e}$ and τ derived for the corona in the case of a plane parallel geometry are not in agreement with the predictions for a simple two phase disk–corona system in energy balance, even under the extreme assumption that all the available gravitational power is dissipated in the hot corona (Haardt & Maraschi 1991, 1993; Stern et al. 1995a). They instead suggest that the hot gas is *photon starved*, i.e., it is undercooled with respect to theoretical expectations based on a stationary equilibrium hypothesis.

Indeed, the fits obtained with a hemispherical model (cf. Fig. 4) yield parameters in agreement with theoretical predictions for this geometry under the same assumptions mentioned above. In fact, a hemisphere

is naturally photon starved with respect to an (infinite) plane parallel system, because of "side effects", which are obviously negligible when the scale height of the corona is much lower than its radial dimension. In any case the best fit values of kT_e are, in the two geometries, roughly consistent, while there is a factor of 2 of difference between the corresponding values of τ (on this point, see section 2).

In the hemisphere case, however, we obtain a large normalization of the reflection component, in excess of unity (again, see section 2 and Fig. 1 on this point), which does not agree with the observed EW of the Fe line, while the slab geometry gives a slightly better fit with a reflection of order unity, as expected. These results indicate that the real model is probably more complicated but not too far from these two ideal cases.

Our results indicate that the anisotropy break should be as expected for the slab but the Comptonization parameter should be higher, as expected for the hemisphere. These two aspects could be reconciled if a significant fraction of the area below a flattish corona *did not* contribute to absorb and reprocess the downscattered Comptonized photons into soft luminosity. One could envisage a picture in which the corona extends down to the very innermost orbits around the black hole, while the inner part of the disk, could be hot and highly ionised. In this kind of picture the average energy balance is shifted toward a photon starved condition, while most of the reflection features from the external part of the disk should be visible anyway. Detailed calculations are necessary to test such kind of picture. A model along this line has been proposed by Belloni et al. (1997) for GRS 1915+105, and is believed to be relevant in the context of the different spectral states observed in Galactic black holes (see, e.g., Narayan, Mahadevan & Quataert 1998).

5.2. Variability

As already discussed, the source exhibits a flare in the central part of the observation during which the X-ray spectrum steepens. Analysing the spectral variability in terms of anisotropic Comptonization models, we find that, irrespective of geometry (see section 3.3, and figure 6), the best fit parameters for the low–to–high state suggest a change of the Compton parameter y, in the sense that y tends to decrease in the high state (cf. Fig. 7). A decrease of y implies a decrease of the Comptonized to soft luminosity ratio.

Since the X–ray continuum varies more at lower energies, pivoting at the highest energies, where the bulk of the Comptonized luminosity is emitted, the change in y is most likely due to an increase of the cooling, rather than to a decrease of the heating. In fact if the heating decreased while the cooling remained constant the pivot should occur at the lowest energies. If this interpretation is correct, then the spectral softening in the high state is naturally explained by a drop of the coronal temperature, ultimately due to an

increase of the EUV soft photon flux. In fact our fits yield lower temperatures of the corona in the higher state and are consistent with the optical depth remaining constant in the transition. More precisely, from the high and low state fits we estimate a Compton parameter of $\simeq 1.3$ and $\simeq 0.6$ in the low and high states respectively, corresponding within the model to an increase of the soft photon luminosity of a factor $\simeq 3$. It is worth noting that similar variability amplitudes have been observed by EUVE in this source on a time scale of a few tenths of kiloseconds, while the 2-10 keV flux was varying by about 20% (Chiang et al., 2000).

We show in Fig. 9 the full best fit models of the low and high state including the soft photon component but removing the neutral absorption and Oxygen edges for clarity. It is remarkable that the required soft luminosities compare well with the intensity and variability range of the UV spectra observed with IUE and shown in Fig. 8. They require however, especially in the case of the softer state, regions of higher temperature than visible in the UV range. It is interesting to recall that Reynolds (1997), fitting ASCA data of NGC 5548 found a significant soft excess with black body temperature near 240 eV and a spectral index of the continuum of 1.9 in the 2–10 keV range, definitely steeper than during this *Beppo*SAX observation. The above soft component could be the signature of the UV-EUV seed photon becoming prominent enough to be directly detected. The corresponding strong cooling of the corona would then imply a steeper X-ray continuum in the ASCA data as observed.

Qualitatively, the spectral and luminosity change can be explained assuming that, in the H (soft) state, the disk pushes a bit closer to the black hole, increasing the portion of the hot corona which "sees" a copious flux of UV–EUV soft radiation. This would cause a more effective cooling of the hot gas, a decrease in its temperature, while the overall energetics would not change substantially. A clear prediction is that the temperature of the soft photons and the strength of the reflection features should be larger in the H state with respect to the L state. Our data are consistent with such a view, and, again, detailed calculations are necessary to test the model quantitatively.

Interpreting variability in terms of the physical parameters obtained with PEXRAV leads to different conclusions. In this case the Compton parameter is consistent with remaining constant between L and H. The decrease of the optical depth is thus expected to go with an increase of the temperature, in agreement with the best fit values. It is however difficult to predict the corresponding change of the soft photon flux.

5.3. The role of pairs

It is interesting to ask what could be the role of electron positron pairs in a corona with the derived parameters. This is determined by the "compactness" parameter $\ell_{\rm X}$.

For any given temperature, there exists a maximum value that $\ell_{\rm X}$ can have, without violating pair equilibrium, i.e., pair production balanced by pair annihilation (Haardt & Maraschi 1993; Svensson 1996). Such limit compactness is reached in the case of a *pure pair* plasma, a situation in which the pair production is so intense that the new created particles dominates the scattering opacity against "normal", pre–existing electrons. A further increase of $\ell_{\rm X}$ would produce more pairs than annihilate, increasing the net opacity of the source, and hence the cooling. The plasma can find a new equilbrium only at a lower temperature.

We can estimate the compactness of NGC 5548 from the luminosity ($L_{\rm X} \simeq 10^{44}$ erg s^{-1}), and from the variability time scale. The variation observed during the *Beppo*SAX long look gives an upper limit of $\sim 3 \times 10^{15}$ cm to the linear dimensions of the varying region. From these values we derive a compactness

$$\ell_{\rm X} \equiv \frac{L_{\rm X}\sigma_{\rm T}}{R m_{\rm e} c^3} \simeq 0.1. \qquad (4)$$

Such value is below the maximum allowed for a slab or hemisphere corona with a temperature ~ 250 keV, assuming energy balance (Stern et al. 1995b), which is of the order of the unity. For this compactness and this temperature the optical depth associated with pairs in equilibrium is smaller than that estimated from our model fits. However, our estimate of the source dimension is probably a rough upper limit, which translates into a lower limit for the compactness. A higher compactness allows for more pairs.

In view of these uncertainities, we can only conclude that a pair dominated corona is not required for NGC 5548.

6. Conclusions

The aim of this paper was to test realistic Comptonization models over the high signal to noise *Beppo*SAX observations of NGC 5548 (which has been detailed by N99). Our main effort was to adopt detailed Comptonization codes that treat carefully the Compton processes in different geometries, especially for what concerns the possible anisotropy of the soft photon field. This last point is crucial, since, in geometries like slabs or hemispheres, the observed first order scattering humps is highly reduced in comparison to the others, producing an anisotropy break just above the averaged energy of twice scattered photons. Specifically, the

*Beppo*SAX observation of NGC 5548 has allowed us to show that:

- the data are well fitted by a plane parallel corona model with an inclination angle of 30° and a soft photon temperature between 5 and 15 eV. The corresponding best fit values of the hot plasma temperature and optical depth are $kT_{\rm e} \simeq 250$ keV and $\tau \simeq 0.1$ respectively. These values of $kT_{\rm e}$ and τ are however not in agreement with a radiatively balanced two phases disk/corona system in plane parallel geometry, even under the assumption that all the gravitationnal power is dissipated in the hot corona. Instead the data suggest that the hot Comptonizing gas is photon-starved. A better agreement is effectively obtained with a hemispherical geometry, which is naturally undercooled with respect to the slab model. However for the hemisphere the anisotropy break is larger, yielding a large reflection component (R=1.6±0.3). This suggests that the real configuration is probably more complex than these two ideal cases.

- the flare occurring during the central 70 ks part of the run enabled us to interpret the spectral change of the source between different states in terms of changes in the physical parameters of the system. Within the framework of anisotropic thermal Comptonisation the change of state suggests a variation of the Compton parameter y, and thus a change of the central configuration. The spectral variability can be most naturally explained by an increase of the soft photon flux causing a reduction of the coronal temperature. be the first

- the zero order cut–off power law approximation commonly used to Comptonization spectra leads to quite different results. The corresponding best fit values of the temperature and optical depth of the corona are $kT_e \simeq 60$ keV and $\tau \simeq 2.4$. The bright state is consistent with the Compton parameter remaining constant during the spectral transition, but suggets an *increase of the coronal temperature* and a *decrease of the optical depth*. This model is statistically acceptable.

- We expect that the substantial improvements in the spectral data at low and medium X-ray energies achievable with CHANDRA and XMM-Newton could discriminate between these alternative models if complemented by simultaneous measurements at higher energies possibly provided by *Beppo*SAX . A decisive progress could come from improved soft γ–ray observations like those expected in the near future by INTEGRAL,

Acknowlegements: We gratefully acknowledge J. Poutanen for providing us his code and the anonymous referee for his helpful comments. POP, FH and LM were supported by the European Commission under

contract number ERBFMRX-CT98-0195 (TMR network "Accretion onto black holes, compact stars and protostars") and by the Italian Ministry for University and Research (MURST) under grant COFIN98-02-154100. GM and GCP were supported by the Ministry for University and Research (MURST) under grant COFIN98-02-32.

REFERENCES

Arnaud, K. A. 1996, ASP Conf. Ser. 101: Astronomical Data Analysis Software and Systems V, 5, 17

Belloni, T., Mendez, M., King, A. R., Van Der Klis, M. & Van Paradijs, J. 1997, ApJ, 488, L109

Boella, G., et al. 1997, A&AS, 122, 327

Clavel, J., et al. 1992, ApJ, 393, 113

Chiang, J., Reynolds, C. S., Blaes, O. M., Nowak, M. A., Murray, N., Madejski, G., Marshall, H. L. & Magdziarz, P. 2000, ApJ, 528, 292

Done, C., Pounds, K. A., Nandra, K. & Fabian, A. C. 1995, MNRAS, 275, 417

Dove, J. B., Wilms, J. & Begelman, M. C. 1997, ApJ, 487, 747

Fiore, F. Guainazzi, M. and Grandi, P. 1999, SAXabc, vs. 1.2, Cookbook for BeppoSAX NFI Spectral Analysis

Frontera, F., Costa, E., Dal Fiume, D., Feroci, M., Nicastro, L., Orlandini, M., Palazzi, E. & Zavattini, G. 1997, A&AS, 122, 357

George, I. M. & Fabian, A. C. 1991, MNRAS, 249, 352

Ghisellini, G. & Haardt, F. 1994, ApJ, 429, L53

Haardt, F. & Maraschi, L. 1991, ApJ, 380, L51

Haardt, F. 1993, ApJ, 413, 680

Haardt, F. & Maraschi, L. 1993, ApJ, 413, 507

Haardt, F. 1994, PhD dissertation, SISSA, Trieste (H94)

Haardt, F. , Maraschi, L. & Ghisellini, G. 1997, ApJ, 476, 620

Iwasawa K. et al., astro-ph/9904071

Jourdain, E., et al. 1992, A&A, 256, L38

Liang, E. P. T. & Price, R. H. 1977, ApJ, 218, 247

Lightman, A. P. & Zdziarski, A. A. 1987, ApJ, 319, 643

Lightman, A. P. & White, T. R. 1988, ApJ, 335, 57

Magdziarz, P. & Zdziarski, A. A. 1995, MNRAS, 273, 837

Magdziarz, P. , Blaes, O. M., Zdziarski, A. A., Johnson, W. N. & Smith, D. A. 1998, MNRAS, 301, 179 (M98)

Maisack, M., et al. 1993, ApJ, 407, L61

Malzac, J., Jourdain, E., Petrucci, P. O. & Henri, G. 1998, A&A, 336, 807

Matt, G., Perola, G. C. & Piro, L. 1991, A&A, 247, 25

Matt, G., Proceeding of the conference "X-ray Astronomy '999. Stellar Endpoints, AGN and the Diffuse Background", September 6-10, Bologna, Italy. To appear in Astrophysical Letters and Communications

Mushotzky, R. F., Fabian, A. C., Iwasawa, K., Kunieda, H., Matsuoka, M., Nandra, K. & Tanaka, Y. 1995, MNRAS, 272, L9

Nandra, K., Pounds, K. A., Stewart, G. C., George, I. M., Hayashida, K., Makino, F. & Ohashi, T. 1991, MNRAS, 248, 760

Nandra, K., George, I. M., Mushotzky, R. F., Turner, T. J. & Yaqoob, T. 1997, ApJ, 477, 602

Narayan, R., Mahadevan, R. & Quataert, E. 1998, Theory of Black Hole Accretion Disks, 148

Nicastro et al., 1999, ApJ, in press (N99)

Parmar, A. N., et al. 1997, A&AS, 122, 309

Poutanen, J. & Svensson, R. 1996, ApJ, 470, 249 (PS96)

Pozdniakov, L. A., Sobol, I. M. & Siuniaev, R. A. 1976, Soviet Astronomy Letters, 2, 55

Reynolds, C. S., Fabian, A. C. & Inoue, H. 1995, MNRAS, 276, 1311

Reynolds, C. S. 1997, MNRAS, 286, 513

Rybicki, G. B. & Lightman, A. P. 1979, New York, Wiley-Interscience, 1979. 393 p.,

Shapiro, S. L., Lightman, A. P. & Eardley, D. M. 1976, ApJ, 204, 187

Stern, B. E., Poutanen, J. , Svensson, R. , Sikora, M. & Begelman, M. C. 1995, ApJ, 449, L13

Stern, B. E., Begelman, M. C., Sikora, M. & Svensson, R. 1995, MNRAS, 272, 291

Suniaev, R. A. & Titarchuk, L. G. 1980, A&A, 86, 121

Svensson, R. 1996, A&AS, 120, C475

Titarchuk, L. 1994, ApJ, 434, 570

Walter, R. & Courvoisier, T. J. -L. 1990, A&A, 233, 40

White, T. R., Lightman, A. P. & Zdiziarski, A. A. 1988, ApJ, 331, 939

Zdziarski, A. A. k. a. 1994, Fabian, A. C., Nandra, K., Celotti, A., Rees, M. J., Done, C., Coppi, P. S. & Madejski, G. M. 1994, MNRAS, 269, L55

This manuscript was prepared with the AAS LaTeX macros v4.0.

Figure Captions

Fig. 1.— Comptonized models for different geometries assuming kT_e = 360 keV and kT_{bb}=5 eV. The slab, hemisphere and sphere geometries are plotted in solid, dashed and dot-dashed line respectively. For the spherical geometry, the soft photons are supposed to be emitted isotropically at the centre of the sphere, whereas they come from the bottom plane for the slab and the hemisphere. The optical depths, chosen so as to produce approximately the same spectral index for $E \lesssim 10$ keV, are 0.09, 0.16 and 0.33 for the slab, hemisphere, and sphere geometry, respectively. For comparison, we have also over-plotted a cut–off power law with $E_{\rm c} = 2kT_{\rm e}$ in dotted line.

Fig. 2.— LECS, MECS and PDS count rate best fit spectra of NGC 5548 obtained with a slab (for 2 inclination angles i=30° and 60°) and a hemisphere (for i=30°) configuration. The corresponding best fit values of kT_{bb}, R, τ and kT_e are reported in Table 1. The ratio between the data and the model is shown in the bottom plot of each figure

Fig. 3.— Contour plots (confidence levels of 68%, 90%, and 99%) of a) τ vs. kT_{bb}, b) kT_e vs. kT_{bb}, c) τ vs. kT_e and d) R versus kT_e for the slab geometry. In Fig. 3c we have over–plotted the expected relation in case of a slab Comptonizing region in energy balance (solid rectangle, solid line, from Stern et al. 1995a) as well as curves of constant Compton parameter in dot-dashed line.

Fig. 4.— Contour plots as in Fig.3 but for the hemispherical configuration. In Fig. 4c we have over–plotted the expected relation in case of a hemispherical Comptonizing region in energy balance (solid hemisphere, dashed line, from Stern et al. 1995a) as well as curves of constant Compton parameter in dot-dashed line.

Fig. 5.— LECS, MECS and PDS spectra of the low (upper panel) and high (lower panel) states of NGC 5548 together with the best fitted Comptonization model for a slab configuration. The corresponding best fit values of kT_{bb}, R, τ and kT_e are reported in Table 2. The ratio between the data and the model is shown in the bottom plot of each figure

Fig. 6.— Confidence levels (68%, 90%, and 99%) for two parameters (kT_e and τ) for the low and high state for the slab (top and bottom left) and the hemisphere (top and bottom right) configuration. In a) and b), the soft temperature kT_{bb} was let free to vary (and the best fit values are indicated by a +), whereas in c) and d) it is fixed to the extreme values allowed by the fit (reported on the figures). As in Fig. 3 and 4,

we have also over–plotted, for both geometries, the kT_e–τ relation predicted for a corona in energy balance (from Stern et al. 1995a).

Fig. 7.— Best fit values of kT_e and τ derived with different models. Triangles and circles represent the results for anisotropic Comptonization models in the slab and hemisphere geometries respectively. Squares represent the values of kT_e and τ obtained with PEXRAV fits (see text for details). Filled symbols refer to the high state, empty symbols to the low state. We have over-plotted the $kT_e - \tau$ relations predicted when energy balance is achieved (solid line for slab, and dashed line for hemisphere; from Stern et al. 1995a). The axis are in logarithmic scales.

Fig. 8.— The full deconvolved *Beppo*SAX spectrum of NGC 5548 in the low state together with non–simultaneous IUE and OSSE data. We have over–plotted the corresponding best fits obtained with an anisotropic Comptonization model (slab geometry) – solid line – and a simple cut–off power law model – dashed line. The IUE data have been fit with a multiple blackbody accretion disk (cf. section 4.1). The vertical line represents the dispersion of the UV fluxes of NGC 5548 measured with IUE between 1983–1995. For clarity, SAX PDS data are plotted with filled circles and the OSSE ones with triangles. The IUE and OSSE data are from M98.

Fig. 9.— Intrinsic model spectra including the required soft blackbody component for the low (dashed line) and high (solid line) states obtained from spectral fits with Comptonization models (slab geometry). The corresponding best fit values of kT_{bb}, R, τ and kT_e are reported in Table 2 . Galactic and warm absorption features have been removed.

Geometry	Inclination	kT_{bb}(eV)	kT_e(keV)	τ	Γ	R	χ^2/dof
Slab	30°	16^{+2}_{-9}	260^{+50}_{-20}	$0.16^{+0.02}_{-0.04}$	-	0.9±0.2	133/168
	60°	25^{+2}_{-3}	210^{+20}_{-20}	$0.33^{+0.07}_{-0.04}$	-	0.6±0.2	168/168
Hemisphere	30°	14^{+2}_{-8}	250^{+70}_{-20}	$0.37^{+0.06}_{-0.11}$	-	1.6±0.3	139/168
Sphere	-	8^{+4}_{-3}	280^{+16}_{-4}	$0.44^{+0.05}_{-0.02}$	-	0.2±0.08	177/168
PEXRAV	-	-	60^{+25}_{-10}	$2.4^{+0.3}_{-0.5}$	$1.59^{+0.01}_{-0.02}$	0.5±0.2	153/169

Table 1: Best fit values of kT_{bb}, kT_e, τ and the reflection normalization R, for different values of the inclination angle i = acos(μ) and for different geometries. For comparison, we also show the best fit values obtained with PEXRAV. We assume in this case $kT_e = E_c/2$ and we compute τ as explained in section 3.2.

State	Geometry	kT_{bb}(eV)	kT_e(keV)	τ	Γ	R	χ^2/dof
Low	Slab	8^{+10}_{-4}	330^{+70}_{-80}	$0.12^{+0.08}_{-0.04}$	-	0.9±0.2	82/113
	Hemisphere	5^{+12}_{-3}	360^{+80}_{-120}	$0.21^{+0.28}_{-0.06}$	-	1.8±0.3	80/113
	PEXRAV	-	55^{+25}_{-10}	$2.6^{+0.2}_{-0.6}$	$1.55^{+0.02}_{-0.02}$	$0.5^{+0.2}_{-0.2}$	93/114
High	Slab	15^{+2}_{-10}	245^{+55}_{-30}	$0.12^{+0.04}_{-0.05}$	-	1.0±0.4	135/144
	Hemisphere	13^{+2}_{-8}	235^{+65}_{-20}	$0.27^{+0.08}_{-0.11}$	-	2.2±0.5	142/144
	PEXRAV	-	80^{+200}_{-35}	$1.6^{+0.8}_{-1.0}$	$1.71^{+0.03}_{-0.04}$	$0.6^{+0.4}_{-0.4}$	142/145

Table 2: Parameters best fit values of the low and high states for comptonization model in different geometries. We also show the best fit values obtained with PEXRAV (like in Table 1, we assume in this case $kT_e = E_c/2$ and we compute τ as explained in section 3.2). We assume here an inclination angle $i = 30°$.

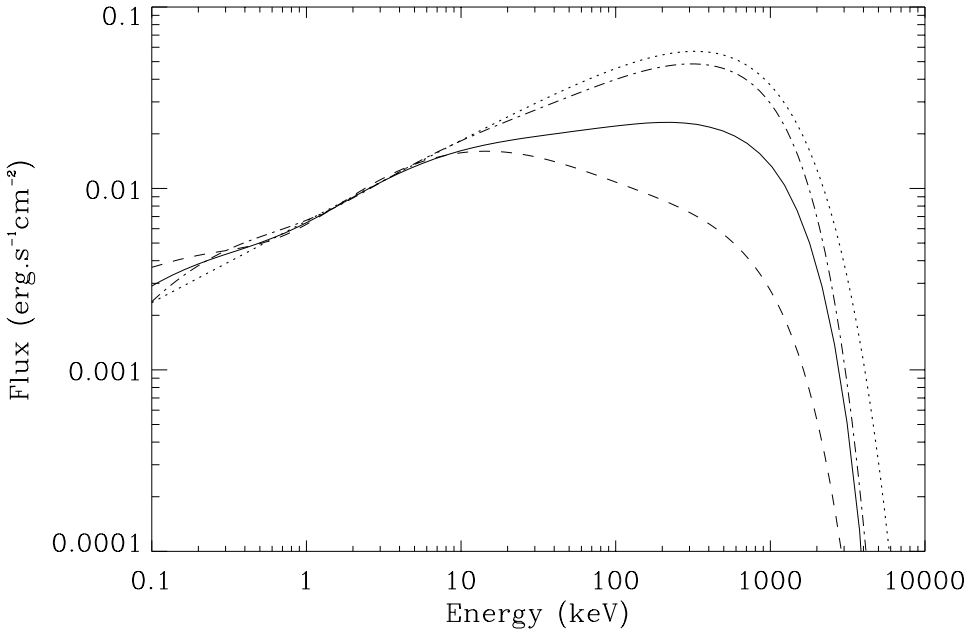
0.1
0.01
0.001
0.0001
Flux (erg.s^{-1}cm^{-2})
0.1
1
10
100
1000
10000
Energy (keV)

Fig. 1.—

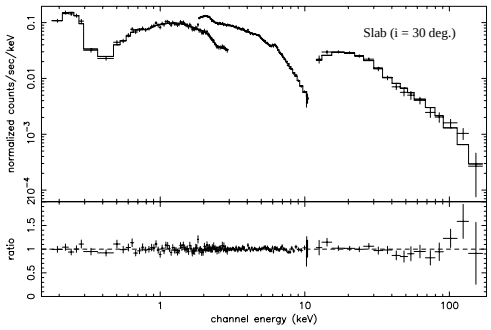
Slab (i = 30 deg.)
normalized counts/sec/keV
ratio
channel energy (keV)

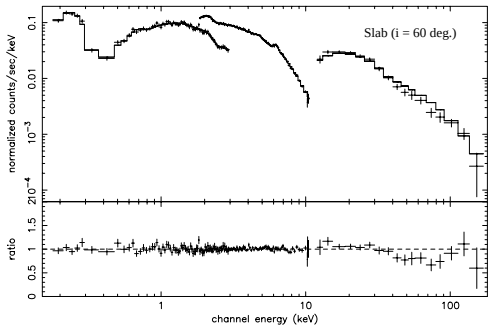
Slab (i = 60 deg.)
normalized counts/sec/keV
ratio
channel energy (keV)

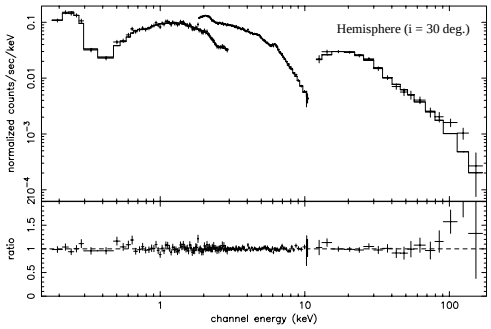
Hemisphere (i = 30 deg.)
normalized counts/sec/keV
ratio
channel energy (keV)

Fig. 2.—

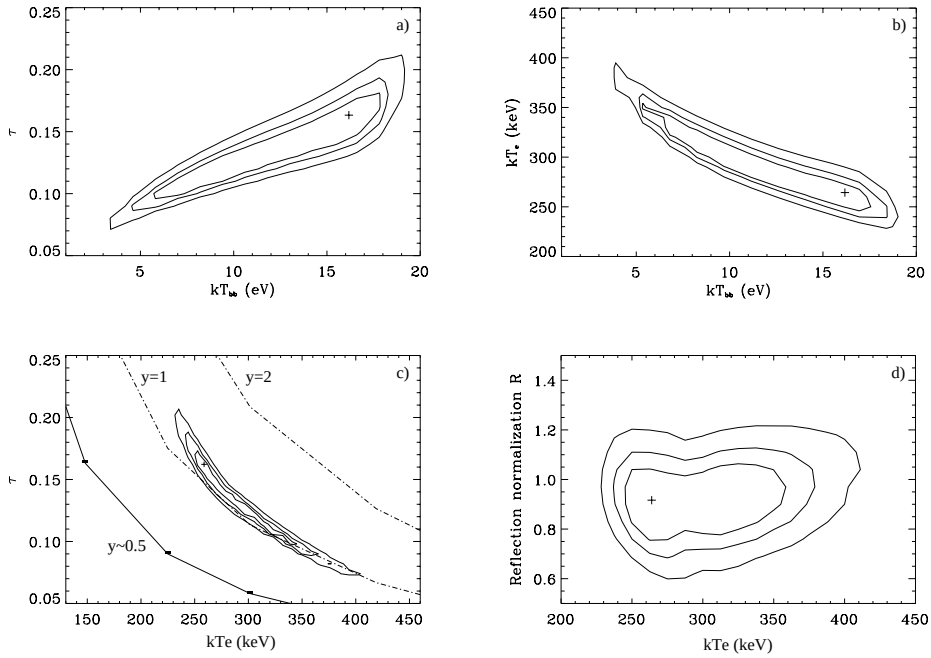
a)
b)
c)
d)
τ
kT_bb (eV)
kT_e (keV)
y=1
y=2
y~0.5
kTe (keV)
Reflection normalization R

Fig. 3.—

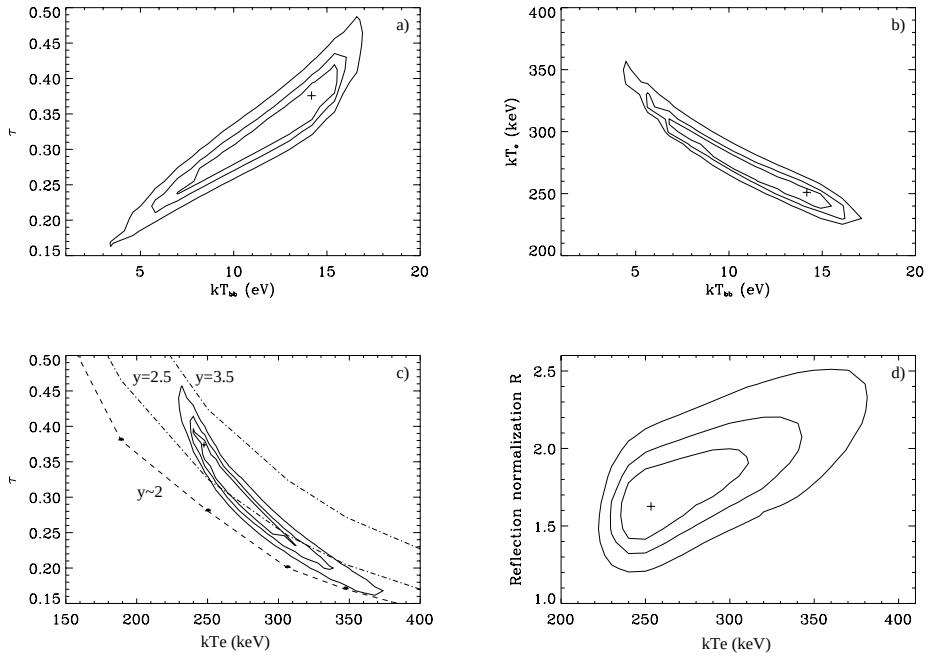
a)
b)
c)
d)
τ
kT_bb (eV)
kT_e (keV)
kTe (keV)
Reflection normalization R
y=2.5
y=3.5
y~2

Fig. 4.—

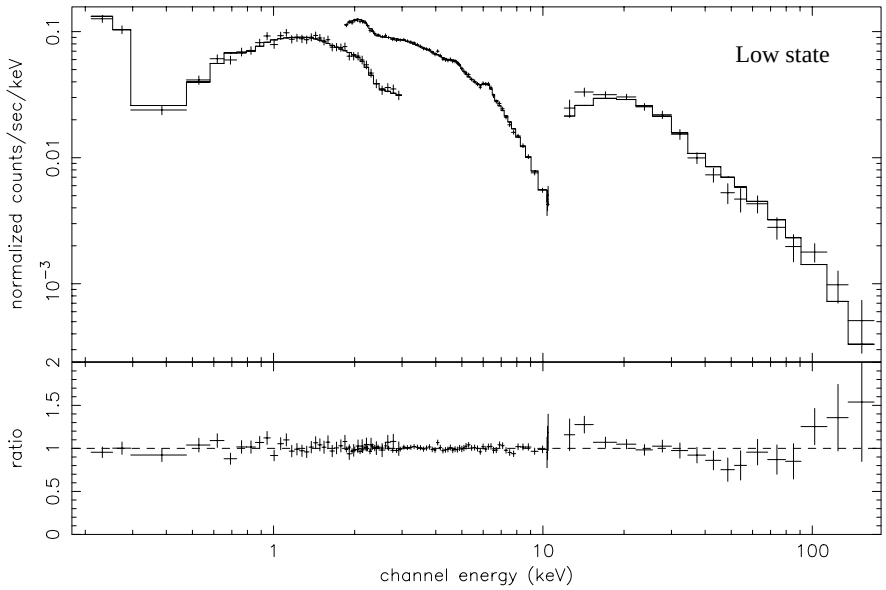
Low state
normalized counts/sec/keV
10^{-3}
0.01
0.1
ratio
0
0.5
1
1.5
2
1
10
100
channel energy (keV)

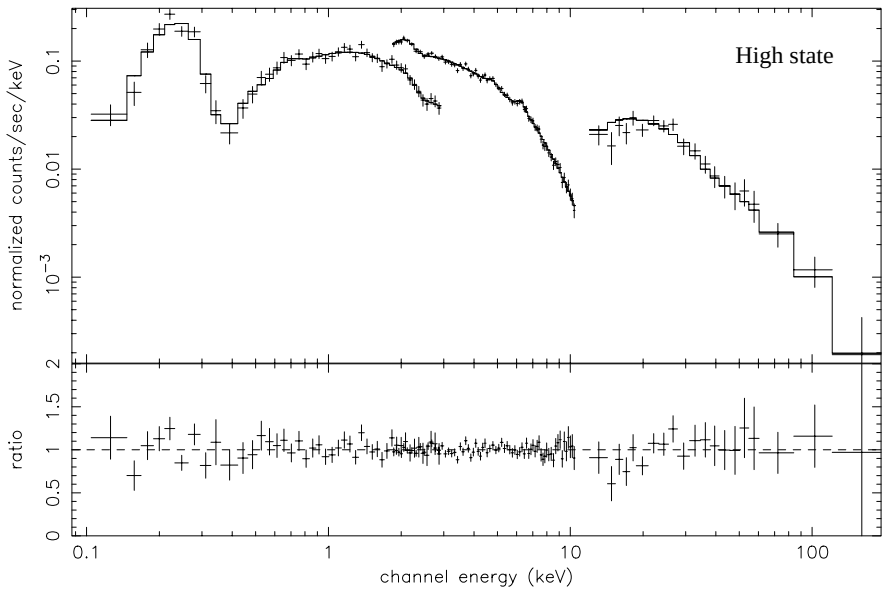
High state
normalized counts/sec/keV
10^{-3}
0.01
0.1
ratio
0
0.5
1
1.5
2
0.1
1
10
100
channel energy (keV)

Fig. 5.—

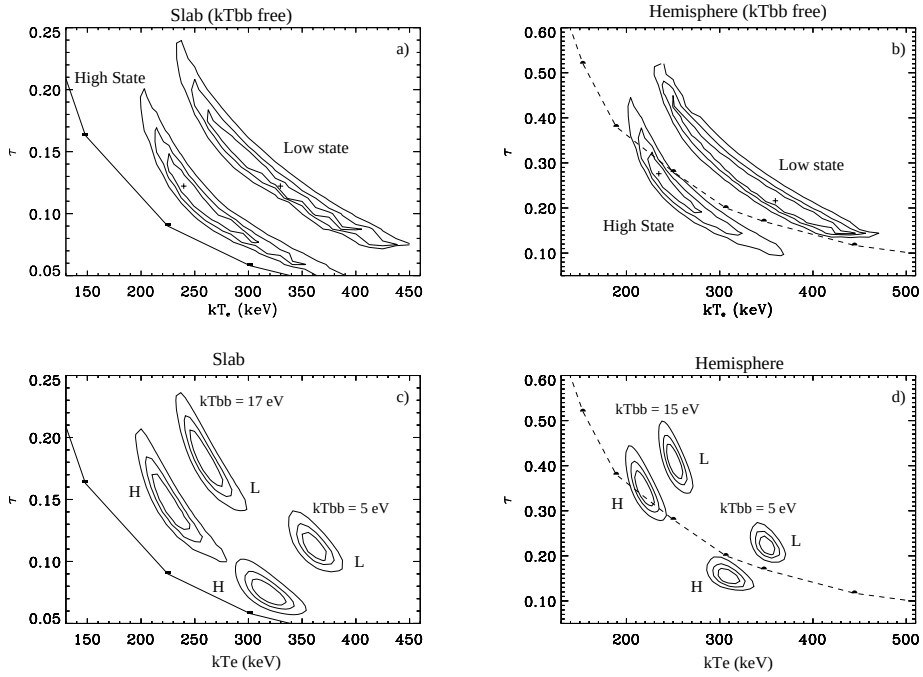
Slab (kTbb free)
a)
High State
Low state
τ
kT* (keV)
Hemisphere (kTbb free)
b)
Low state
High State
τ
kT* (keV)
Slab
c)
kTbb = 17 eV
H
L
kTbb = 5 eV
L
H
τ
kTe (keV)
Hemisphere
d)
kTbb = 15 eV
L
H
kTbb = 5 eV
L
H
τ
kTe (keV)

Fig. 6.—

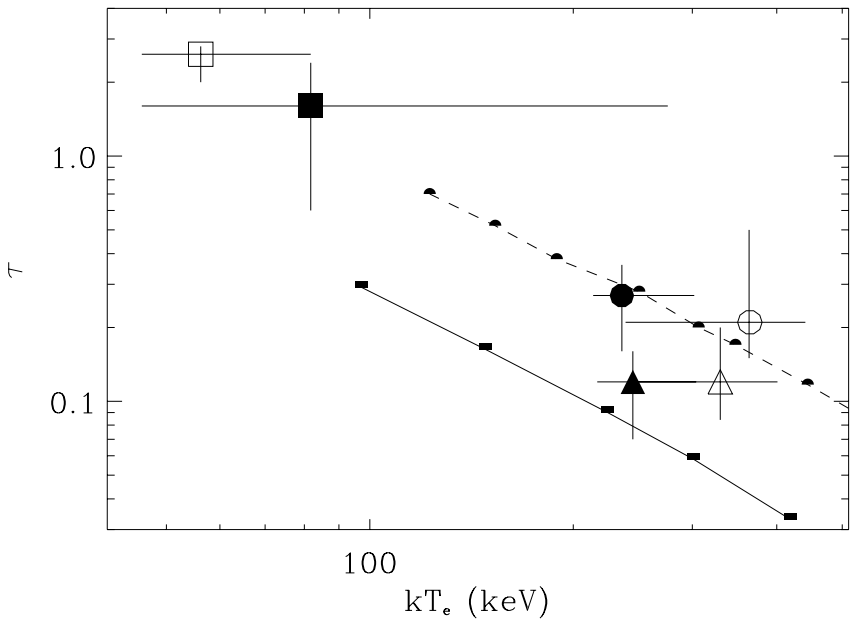

Fig. 7.—

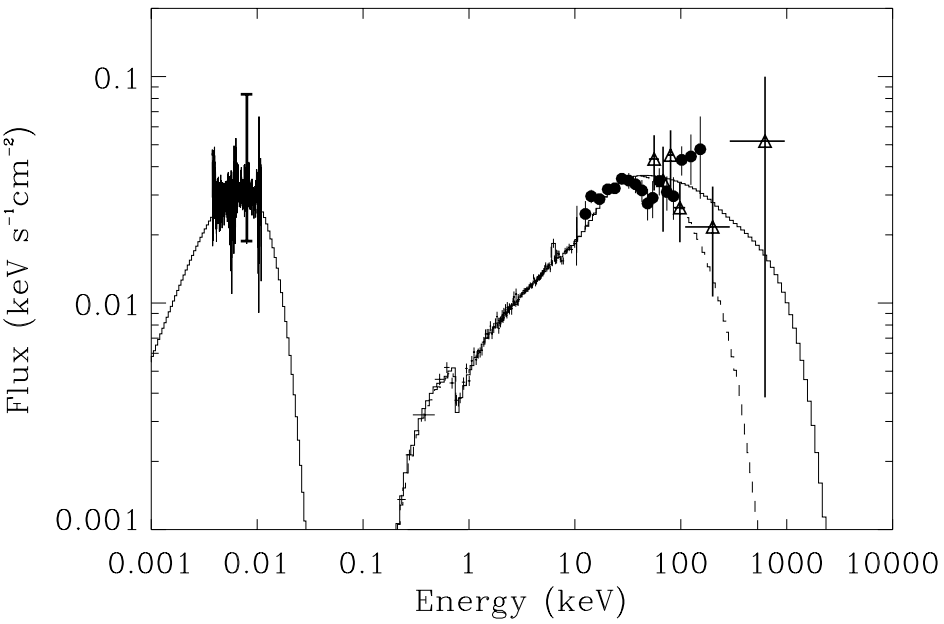
0.1
0.01
0.001
Flux (keV s^{-1}cm^{-2})
0.001
0.01
0.1
1
10
100
1000
10000
Energy (keV)

Fig. 8.—

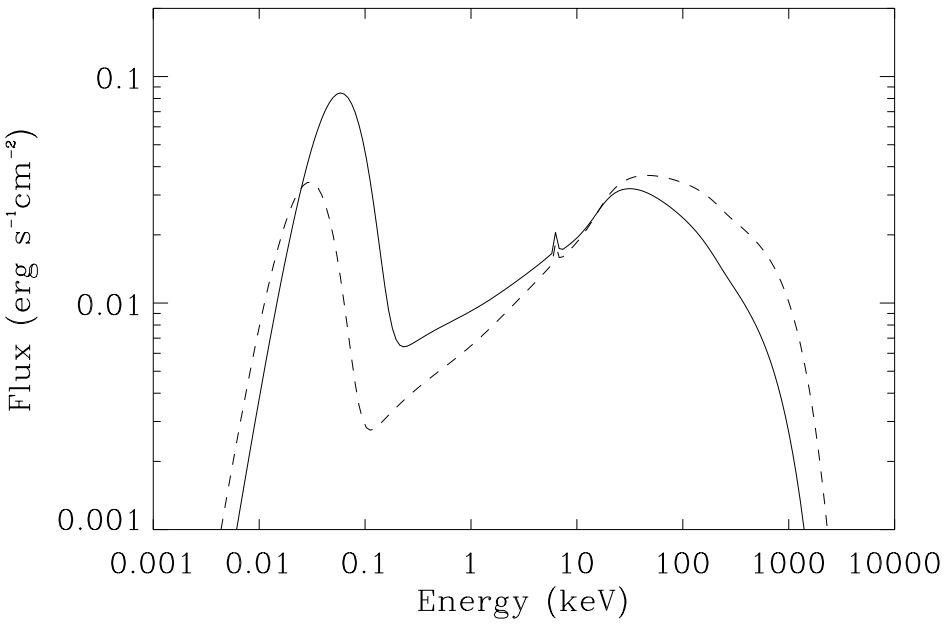
0.1
0.01
0.001
Flux (erg s^{-1}cm^{-2})
0.001
0.01
0.1
1
10
100
1000
10000
Energy (keV)

Fig. 9.—